https://doi.org/10.20965/ijat.2014.p0550

Paper:

Contributions of High-Speed Cutting and High Rake Angle to the Cutting Performance of Natural Rubber

Naoki Takahashi and Jun Shinozuka

Yokohama National University
79-5 Tokiwadai, Hodogaya, Yokohama, Kanagawa 240-8501, Japan
E-mail: {takahashi-naoki-rp, jshinozu}@ynu.jp
[Received March 30, 2014; accepted May 14, 2014]

This study investigates the contributions of high-speed cutting and a high rake angle to the improvement of the cutting performance of natural rubber. Orthogonal cutting experiments were conducted at cutting speeds ranging from 1.0 m/s to 141.1 m/s. The rake angles examined were 0°, 20° and 50°. The following results were obtained from the experiments. The cutting ratio is almost 1.0 regardless of the cutting speed and rake angle. The cutting force rises rapidly as the cutting speed increases. High-speed cutting or a high rake angle eliminates tear defects on the machined surface and reduces chipping defects at the entry edge of the workpiece. An uncut portion, however, always remains at the exit edge. The cross-sectional shape of the machined surface becomes concave. Besides, the machined surface comes into broad contact with the clearance face. These degradations in the shape accuracy arise from the large elastic distortion that occurs in the shear zone. Increasing the cutting speed improves the flatness of the machined surface. Although an analysis of the cutting mechanism reveals that the apparent stiffness of the material in the shear zone is enhanced with increasing the cutting speed, a very high cutting speed worsens the shape accuracy because of the development of shock waves. Depending on the rake angle, there is a critical cutting speed that should not be exceeded to maximize the cutting performance of natural rubber.

Keywords: high-speed cutting, natural rubber, viscous drag, cutting force, shape accuracy

1. Introduction

Natural rubber, which is widely used in a variety of industrial parts, exhibits viscoelastic behavior. A part made of natural rubber is typically manufactured using an injection molding process with a metal mold. This process is economical for mass production. The cost of this process, however, tends to be high for small-scale production because the machining cost for a metal mold is typically high. In order to provide a solution to the problem of high cost of small-scale production, this study investigates the applicability of manufacturing a part made of natural rubber by machining process.

Commercially available black Natural Rubber (NR) contains several chemical substances, such as carbon black, silica, and vulcanization accelerators, and is also formed by mixing many small pieces of reclaimed rubber. The physical and mechanical properties of NR depend on the blending ratio of these substances [1–6]. The typical material properties of NR are characterized as follows: the Young's modulus of NR is much lower than that of metals. The Poisson's ratio of NR is close to 0.5, which means that the volumetric strain is almost zero. Most of the deformation in NR occurs elastically. Hence, the deformation that occurs during loading is recovered elastically soon after loading. In addition, the stress strain behavior of NR is highly dependent on time and the deformation history [7]. In the cutting of NR, these properties pose some problems, such as the propensity for tear defects and chipping defects on the machined surface and the degradation of the accuracy of the machined shape. These problems become more noticeable in the machining of a part with a complex shape.

The use of a cutting tool with a high rake angle can provide a solution to these problems because a high rake angle decreases the degree of deformation in the shear zone [8, 9]. A strategy for strengthening the stiffness of the material has also been examined. Temperature is one of the key factors in the characterization of the material properties of viscoelastic materials. The stiffness of a viscoelastic material increases rapidly when its temperature is below its glass transition temperature. Cryogenic machining has been proposed as an effective approach to take advantage of this behavior in the machining of viscoelastic materials [10–12]. In conjunction with cryogenic methods, a method for restricting the deformation of the free surface with a fixture has also been attempted [13]. The applicability of cutting with a heated tool has also been examined [14], as has been the feasibility of high-speed milling of rubber [15]. The latter study focused on the effect of the increase in the apparent elastic modulus with the loading frequency.

In order to analyze the cutting mechanism of viscoelastic materials, it is very important to grasp the relevant constitutive equation. Many mathematical models for the stress-strain relations of viscoelastic materials have been proposed [16]. These models principally consist of a description of an elastic spring and a viscous dashpot. Because a viscous dashpot generates a drag that depends on the rate of expansion and contraction rate, the apparent stiffness is enhanced as the rate of expansion and contraction increases. If this concept is applied to the cutting process, it is expected that high-speed cutting would improve the machinability of NR at room temperature.

The maximum cutting speed examined in the studies cited above [10–15] was 12.6 m/s. It appears that much higher cutting speeds have not yet been considered. Hence, it is unknown whether a much higher cutting speed provides a greater benefit. The authors have been studying high-speed cutting of various metals using a high-speed impact cutting device that they have developed [17–21]. This tester is an air gun-type device in which a small cutting tool is installed in a lightweight projectile and is accelerated with compressed gas. The maximum cutting speed is 210 m/s.

The present study investigates the influences of high-speed cutting and a high rake angle on the cutting characteristics of NR. Orthogonal cutting experiments were conducted with cutting speeds ranging from 1.0 m/s to 141.1 m/s. In the cutting tests, a shaping machine was utilized for cutting speeds slower than 2 m/s, and a high-speed impact cutting tester was used for cutting speeds faster than 10 m/s. The rake angles examined were 0°, 20° and 50°. In the experiments, the changes in the chip morphology, the shape of the machined surface, and the cutting force with the cutting speed and the rake angle were investigated. The stress field in the shear zone was analyzed by employing a simple shear plane model. This paper presents the results obtained and discusses the contributions of high-speed cutting and a high rake angle to the improvement of the cutting performance of NR.

2. Experimental Setup

2.1. Properties of Workpiece Material

The workpiece was a commercially available black Natural Rubber (NR) sheet of 2 mm in thickness. The Shore A hardness is one of the important material properties of NR. The value of the Young's modulus can be calculated using the Shore A hardness number [22]. From the values of the Young's modulus and the density, the speed of the stress wave that travels in the material can be estimated. The influence of the speed of the stress wave on the cutting characteristics of the material is discussed briefly later. The results of an experiment conducted to measure the hardness of the material using a durometer revealed that the Shore A hardness of the workpiece material was A 69. In the experiment, both the change in the hardness of the material over time at room temperature and the change in the hardness with temperature were investigated. **Fig. 1(a)** shows the change in Shore A hardness number with the elapsed time after loading. The hardness decreased by no more than 2% after 1 s had elapsed. The time during which a material undergoes deformation in the shear zone during cutting is very short less than 10^{-4} s when the depth of cut is 0.2 mm and the cutting speed is 1 m/s. Therefore, the effect of stress relaxation can be ignored in the analysis of the cutting mechanism. **Fig. 1(b)** shows the change in the Shore A hardness with temperature. Each shore hardness number plotted in this figure was measured after the temperature of the material had stabilized. The hardness decreased by approximately 15% when the temperature exceeded the room temperature by 100 K, and then leveled off. The thermal softening effect became weak when the temperature of the material exceeded 400 K.

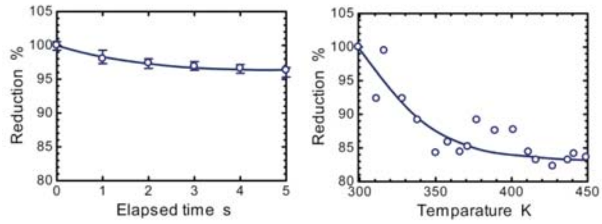

(a) Effect of time (b) Effect of temperature

Fig. 1. Change in Shore A hardness of natural rubber.

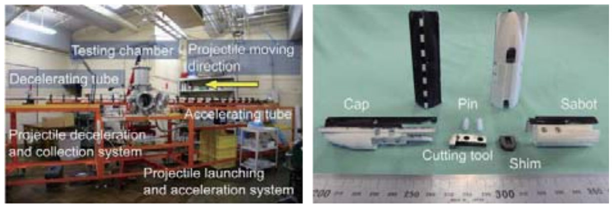

(a) Panoramic view (b) Projectile with cutting tool

Fig. 2. High-speed impact cutting tester used in this study.

2.2. Configuration for High-Speed Impact Cutting Test

In this study, orthogonal cutting tests were conducted at cutting speeds V ranging from 1 m/s to 140 m/s. The depth of cut, t_1, was 0.2 mm. **Fig. 2** shows the apparatus used in the high-speed cutting experiment. **Fig. 2(a)** shows a panoramic view of the high-speed impact cutting tester used, which was developed in previous studies [17–21]. **Fig. 2(b)** shows a projectile with a small built-in cutting tool. The detailed specifications of the tester are described in the literature [17, 19]. The material used in the small cutting tool was P20 tungsten carbide. In this study, three rake angles γ of 0°, 20° and 50° were examined, as shown in **Figs. 3(a)**, **(b)** and **(c)**, respectively. The clearance angle α was fixed at 6°. Both the rake and the clearance faces were ground to form a shape cutting edge with a #1200 diamond wheel before every experiment. **Fig. 3(d)** shows a Scanning Electron Microscopy (SEM) photograph of the cutting edge at a rake angle of 0°. The edge radius was less than 1 μm. Because the depth of cut was 0.2 mm, it was considered reasonable to assume that the influence of the cutting edge radius on the cutting mechanism could be ignored. **Fig. 4(a)** shows the

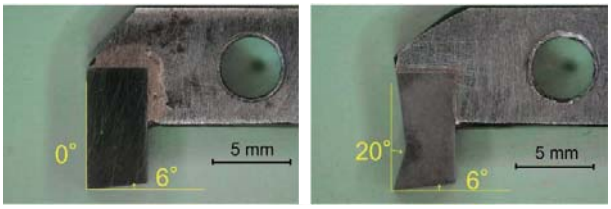

(a) $\gamma = 0°$ (b) $\gamma = 20°$

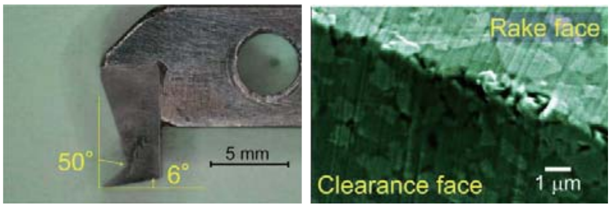

(c) $\gamma = 50°$ (d) Cutting edge (SEM)

Fig. 3. Small cutting tools used.

(a) Whole view (b) Cutting die

Fig. 4. Shape of workpiece.

shape of the workpiece used in the experiment. The shape of the workpiece was formed by a die cutting process using the cutting die shown in **Fig. 4(b)**. The surface to be cut is shown in **Fig. 4(a)**. The width of cut, b, was 2 mm, and the cutting length l_1 was 60 mm. In the cutting experiments conducted with the shaping machine, all of the cutting conditions except the cutting speed were the same as those for the high-speed cutting tests.

2.3. Analysis of Measured Cutting Force

The cutting time is short in high-speed cutting. For example, the cutting time is 428.6 μs when the cutting speed is 140 m/s. **Fig. 5(a)** shows an example of the cutting force measured. In this case, the rake angle was 0° and the cutting speed was 141 m/s. Although the dynamometer system can respond to frequencies of up to approximately 14 kHz [17], the force measured might not be the true force. Therefore, in this study, the true force was estimated using the measured force and the transfer function of the dynamometer system by employing a Fast Fourier Transform (FFT) analysis. The change in the true depth of cut was determined by comparing the shapes of the workpiece before and after cutting, as shown in **Fig. 5(b)**. The two sets of data were combined to calculate the specific forces (uFP and uFT, the cutting force per cutting area) as shown in **Fig. 5(c)**. It should be noted that the shape of the waveform of the specific force differed from that of the measured force because the true depth of cut fluctuated. The details of this analysis method have been described

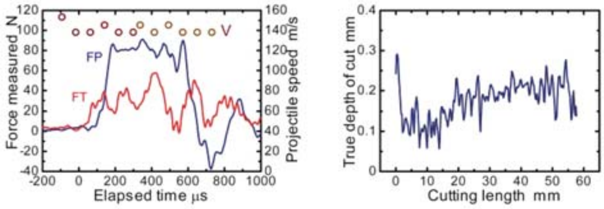

(a) Force and speed measured (b) True depth of cut

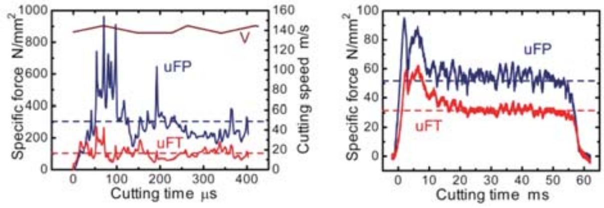

(a) Specific force calculated (d) For $V = 1.0$ m/s

Fig. 5. Analysis of measured cutting force.

in the literature [19].

In this study, the cutting force, shown in **Fig. 14**, was calculated by multiplying the mean value of the estimated specific force with a constant value for the cutting area. The constant value for the cutting area was 0.4 mm^2 ($A = bt_1$). The mean value of the specific force is indicated by the broken lines in **Figs. 5(c)** and **(d)**. **Fig. 5(d)** shows the specific force for a cutting speed of 1.0 m/s. Both the principal force and the thrust force increases as the cutting speed increases, as described later.

3. Results and Analysis

3.1. Experimental Results

Figure 6 shows the chip shapes formed under various cutting conditions. A rake angle of 0° results in a curled chip, whereas rake angles of 20° and 50° result in straight chips. It is worth noting that the length of the chip is almost equal to the cutting length, regardless of the rake angle and cutting speed. This means that the cutting ratio r_c is approximately 1.0 regardless of the rake angle and cutting speed and that most of the shear deformation in the shear zone occurs elastically. The cutting ratio being 1.0 regardless of the cutting speed suggests that the shear angle ϕ can be determined by the rake angle alone, regardless of the cutting speed, as expressed by Eq. (1).

$$\phi = \tan^{-1}\left(\frac{r_c \cos\gamma}{1 - r_c \sin\gamma}\right) \approx \frac{\pi}{4} + \frac{\gamma}{2} \quad . \; . \; . \; . \quad (1)$$

Figure 7 illustrates how the shear angle, which was calculated from the chip length l_2 and the cutting length l_1, changes with the cutting speed. When the rake angle is 0°, a shear angle of approximately 41° is obtained using the least squares method, as indicated by the line in the figure. Similarly, the shear angle is 54° for a rake angle of 20°, and 68° for a rake angle of 50°. These values nearly agree with those indicated by Eq. (1). Therefore, Eq. (1) was used in this study to analyze the cutting mechanism,

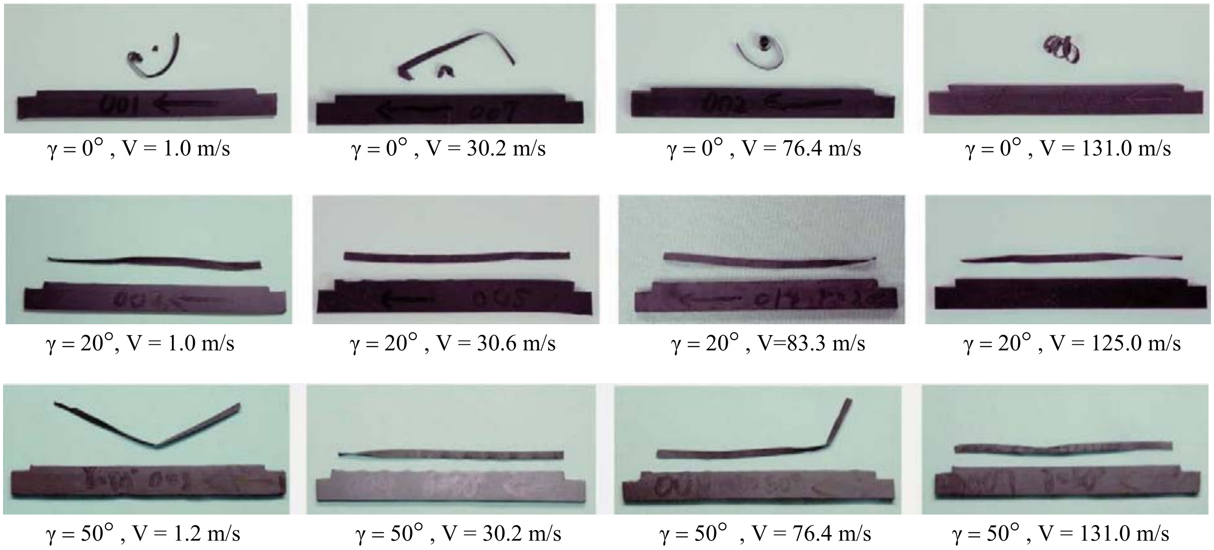

Fig. 6. Photographs of chip and workpiece under various cutting conditions.

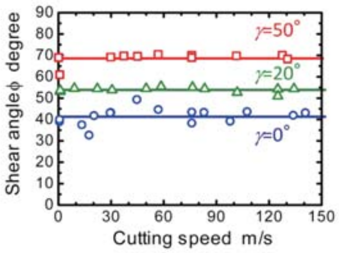

Fig. 7. Changes in shear angle with cutting speed.

as described in a later section.

Typical cutting equations for orthogonal metal cutting indicate that the shear angle ϕ can be estimated using the rake angle γ and the friction angle β [23]. The friction angle β reflects the mean friction at the interface between the rake face and the chip. If these cutting equations are applicable to the cutting of NR, β depends only on γ. Hence, in the cutting of NR, the friction angle β is largely unaffected by the cutting speed.

Equation (1) shows that the cutting speed does not affect the shear strain γ_s on the shear plane. The shear strain γ_s depends only on the rake angle if the simple shear plane model is applicable:

$$\gamma_s = \frac{\cos\gamma}{\sin\phi\cos(\phi-\gamma)} \approx \frac{2\cos\gamma}{1+\sin\gamma} \quad . \; . \; . \; . \quad (2)$$

Figure 8 shows the free surface and back surface of a chip. For a rake angle of 0° and any cutting speed or a rake angle of 20° at a cutting speed of 1 m/s, the width of the chip shrinks slightly. However, in all cases, no significant unevenness or lamella structure, which can be observed in the cutting of metals, can be observed on the free surface of the chip. On the back surface of the chip, both of the side edges are slightly bent up.

Figure 9 shows the morphology of the portion of the workpiece at the entry edge for various rake angles and cutting speeds. At a cutting speed of 1 m/s, chipping defects occurred at the entry edge of the workpiece at rake angles of 0° and 20° but not at 50°. The chipping defects are attributable to crack initiation on the workpiece surface behind the cutting edge as a result of the low material stiffness. Increasing the cutting speed tends to reduce the occurrence of chipping defects, even at a rake angle of 0°. Therefore, stress concentrations at the cutting edge are intensified as the cutting speed increases.

Figure 10 shows the morphology of the portion at the exit edge of the workpiece at various rake angles and cutting speeds. Around the exit edge, there is a portion that has not been cut at all, regardless of the rake angle and cutting speed. The volume of the uncut portion does not seem to decrease even if the rake angle and cutting speed increase. Thus, neither high-speed cutting nor a high rake angle has much effect on reducing the degradation of the shape accuracy around the exit edge of the workpiece.

Figure 11 shows the morphology of the machined surface at various rake angles and cutting speeds. When the rake angle is 0°, tear defects occur on the machined surface at low cutting speeds. However, increasing the cutting speed eliminates tear defects. When the rake angle is 20° or 50°, tear defects do not occur even at a cutting speed of 1 m/s. Under these conditions, small pieces of reclaimed rubber, which can be seen as shiny black spots, were cut. This suggests that large cracks are not initiated at the cutting edge. It is reasonable to assume that chips are formed not by peeling but by viscoelastic shearing. Therefore, a simple shear plane model was employed in this study to analyze the cutting mechanism.

The shape of the machined surface along the width of cut did not become planar in shape under all conditions. This was especially true when the rake angle was 0° and the cutting speed was 131 m/s: a portion near both of the side edges remained without cutting.

Figure 12 shows the shape of the cross section of the machined surface, which is perpendicular to the cutting direction, under various cutting conditions. The cross section was a concave in shape regardless of the rake angle and cutting speed. The middle portion with respect to the

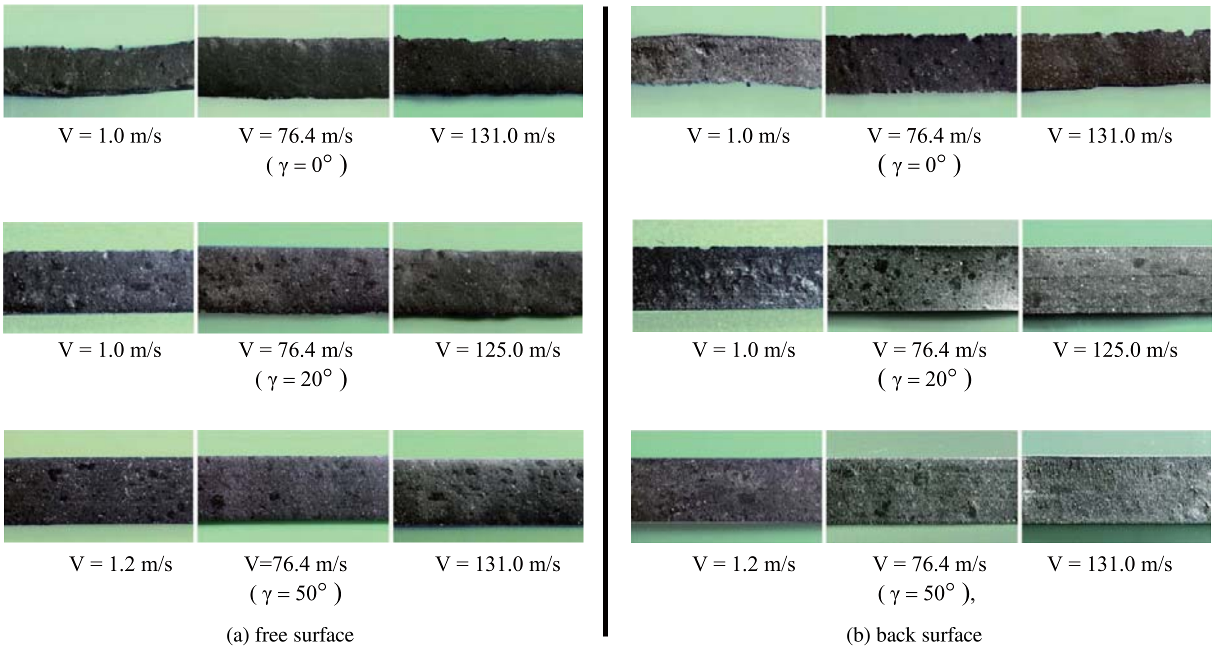

Fig. 8. Morphology of chip under various cutting conditions.

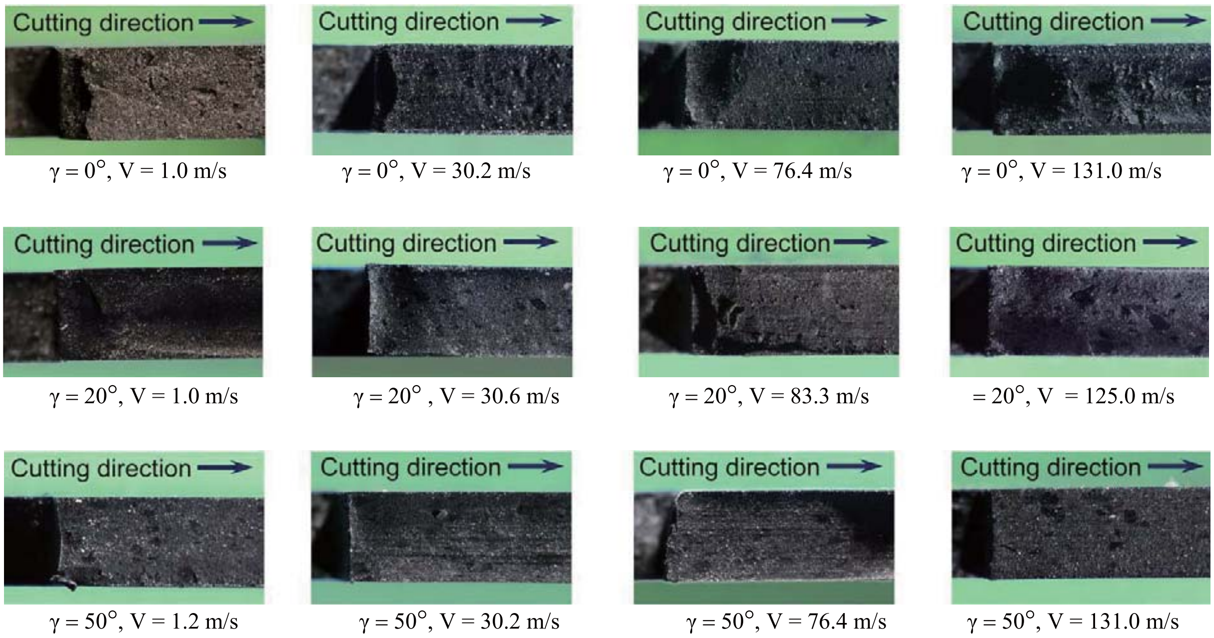

Fig. 9. Morphology of machined surface at the entry edge of the workpiece under various cutting conditions.

width of cut exhibited dents. The mechanism of the formation of the concave shape can be explained as follows. The material ahead of the cutting edge is distorted largely to flow toward the free surface side, in the manner of the formation of a side burr in metal cutting. However, the degree of distortion or deflection for NR or viscoelastic materials is much larger than that for metals. The material near both the free surface sides is forced to move below the cutting edge. Consequently, a portion of the material near both the free surface sides is hardly removed. After the cutting edge passes through, the distortion or deflection is completely recovered elastically. This large elastic recovery after loading is one of the typical properties of viscoelastic materials. Hence, cross section of the machined surface becomes concave in shape. The difference between the peak and the valley of the concave shape becomes small as the rake angle increases. When the rake angle is 50° and the cutting speed is 1.2 m/s, the machined surface is almost flat. Increasing cutting speed also decreases the difference between the peak and the valley of the concave shape. The shape accuracy, however, degrades when the cutting speed exceed a certain speed. When the rake angle is 0°, the difference between the peak and the valley of the concave shape at a cutting

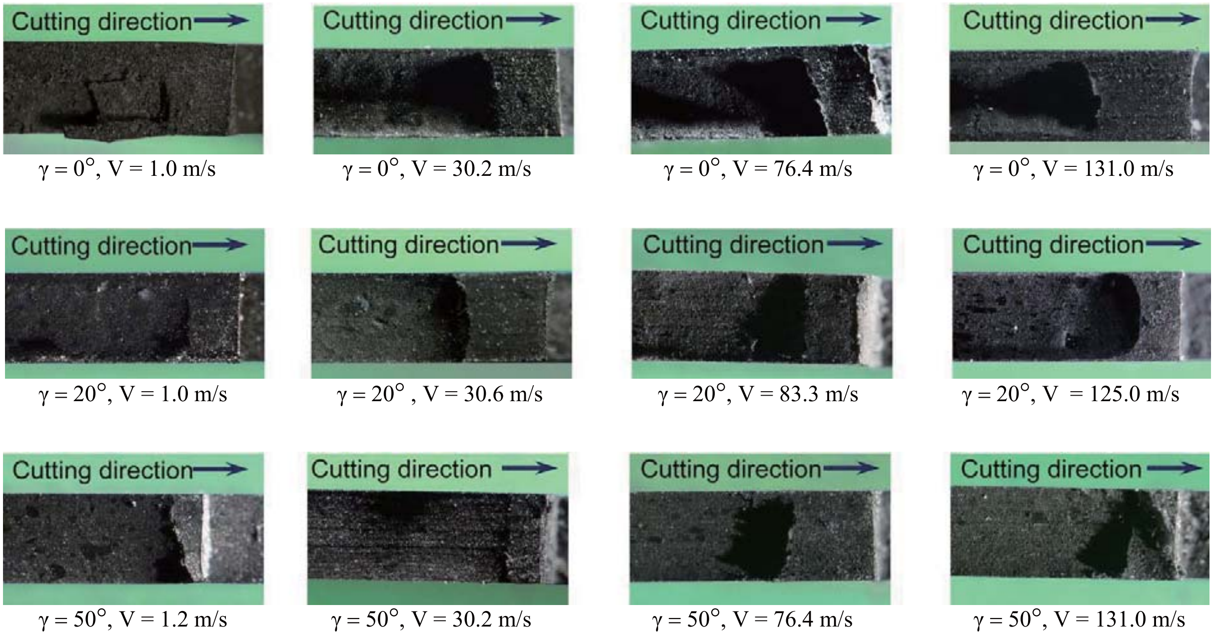

Fig. 10. Morphology of machined surface at the exit edge of the workpiece under various cutting conditions.

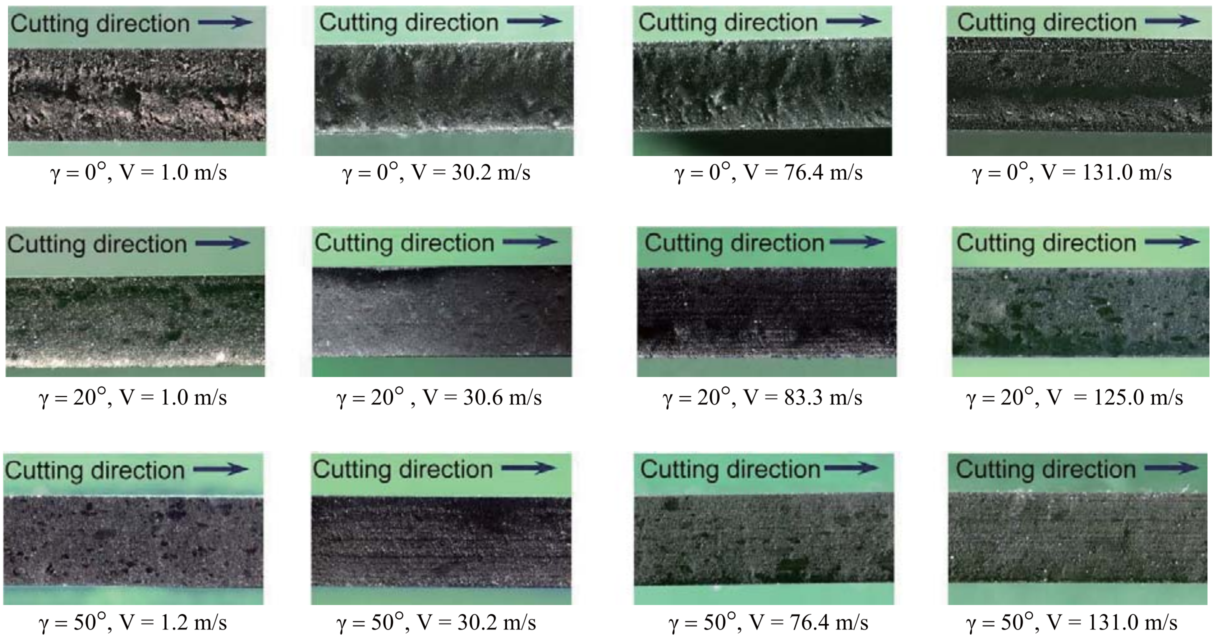

Fig. 11. Morphology of machined surface at the middle over the cutting distance under various cutting conditions.

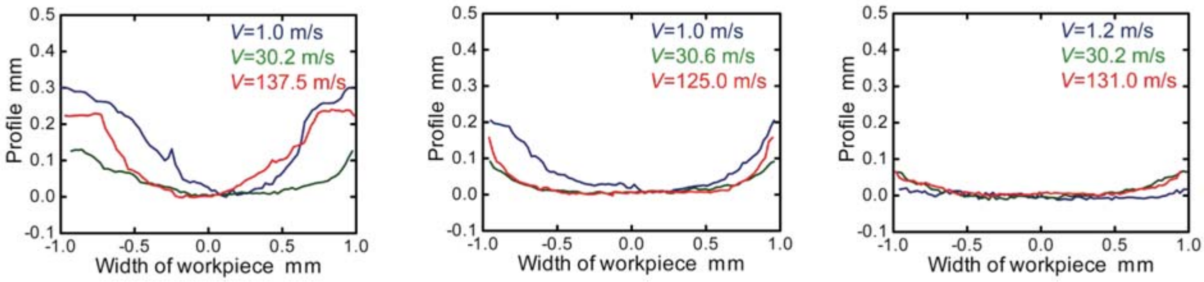

(a) $\gamma = 0°$ (b) $\gamma = 20°$ (c) $\gamma = 50°$

Fig. 12. Cross-sectional shape of machined surface under various cutting conditions.

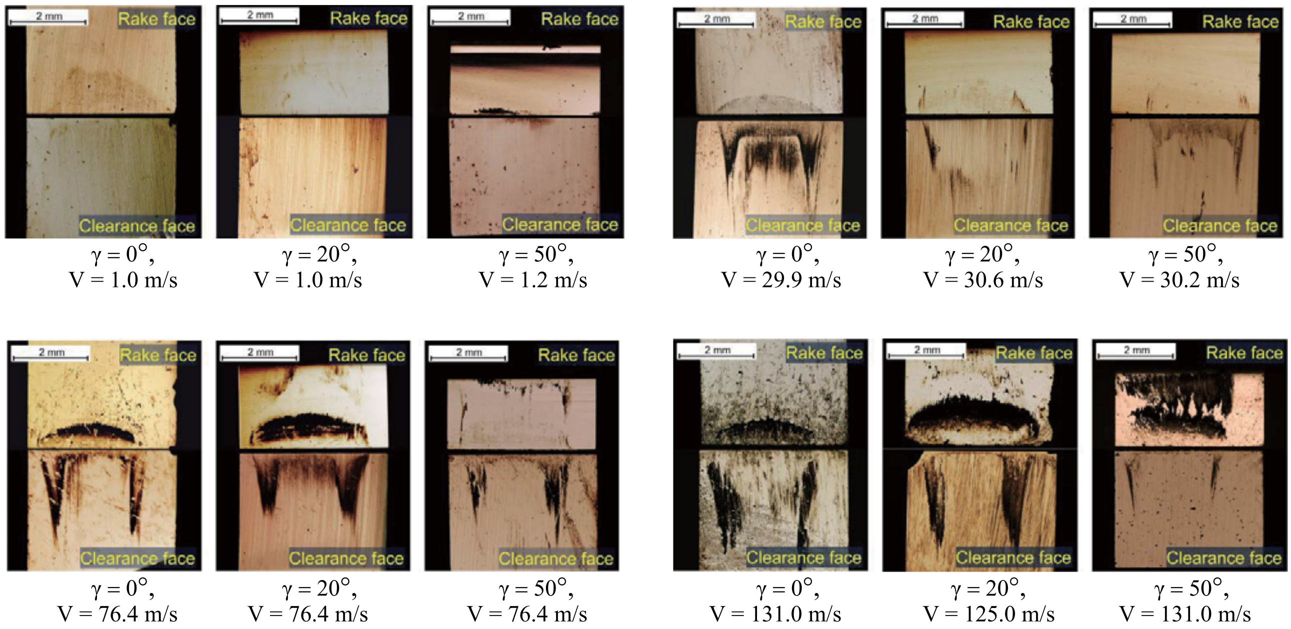

Fig. 13. Appearance of rake face and clearance faces under various cutting conditions.

speed of 1.0 m/s is high and is 0.3 mm, which is 1.5 times the depth of cut. The difference decreases to less than one third when the cutting speed is approximately 30 m/s. When the cutting speed increases further, the difference widens again. Moreover, the surfaces near both of the free surface sides remain uncut when the rake angle is 0° and the cutting speed exceeds 130 m/s.

Figure 13 shows the appearance of the rake and clearance faces after cutting at various rake angles and cutting speeds. The length of the cutting edge is 4 mm. The contact area between the rake face and the chip expands as the rake angle increases at a given cutting speed or as the cutting speed increases at a given rake angle. It is worth noting that the machined surface comes into broad contact with the clearance face in high-speed cutting. For a given cutting speed, the contact area between the clearance face and the machined surface increases as the rake angle decreases, and when the rake angle is 0°, the contact area increases as the cutting speed increases. For the rake angles of 20° and 50°, the contact area at the clearance face does not seem to change under high-speed cutting conditions. The wide contact area between the clearance face and the machined surface is caused by the large elastic recovery, as explained before. The shape of the contact region at the clearance face is strongly related to the concave shape of the machined surface. Besides, the widths of the contact areas for both the rake and the clearance faces are wider than the width of the workpiece (2 mm). These findings reveal that the material in the vicinity of the cutting edge deforms substantially and flows toward both the free surface sides. In additions, the appearance of black substances adhered to the rake and clearance faces implies that the stresses and temperature at the interface between the clearance face and the machined surface is almost the same as those at the interface between the rake face and the chip.

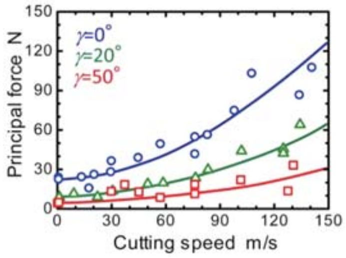

(a) Principal force

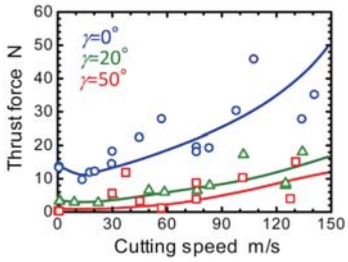

(b) Thrust force

Fig. 14. Changes in cutting force with cutting speed.

Figure 14 shows the changes in the cutting force with the cutting speed and rake angle. The circles indicate the analyzed experimental data as mentioned in section 2.3. The solid curves, representing cutting speed from 1 m/s to 150 m/s, were drawn by interpolation by hand from the discrete experimental data points. The shear stress in the shear zone was calculated using the solid curve. Both the principal force and the thrust force rise rapidly as the cutting speed increases, regardless of the rake angle.

In metal cutting, due to thermal softening effect, the cutting force decreases with cutting speed until the cutting speed reaches a certain speed. However, this phenomenon is not evident in NR cutting, because of the material property of NR, as shown in **Fig. 1(b)**. When the

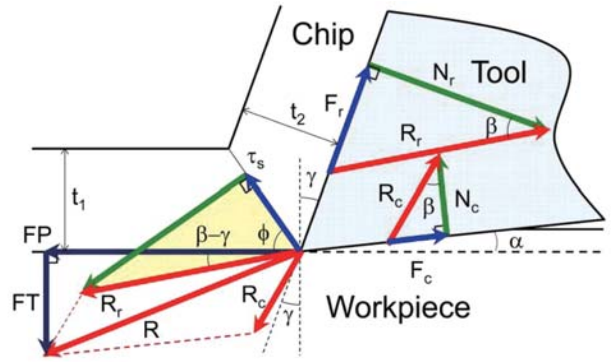

Fig. 15. Cutting model used for analysis.

cutting speed is 150 m/s, the principal force is approximately six times higher than that at a cutting speed of 1 m/s, and the thrust force is approximately three times higher than that at a cutting speed of 1 m/s, regardless of the rake angle. At a rake angle of 50°, the thrust force is more likely to become negative when the cutting speed is less than 30 m/s. Hence, when a higher rake angle is used, it can be seen that the cutting speed should be increased because the negative thrust force makes the cutting state unstable.

3.2. Analysis of Cutting Mechanism

Characterizing the stress field in the shear zone is very important to the analysis of the cutting mechanism and the evaluating of the cutting performance. Various cutting models have been proposed, including a model based on an energy method [24] and a model based on slip-line field theory [25]. The simple shear plane model is widely used to characterize the nature of orthogonal cutting mechanism. Although the cutting state of NR is not completely orthogonal state as understood from **Fig. 13**, the simple shear plane model was employed in this study. The problem associated with applying the model to the analysis of the cutting mechanism of NR is that the machined surface comes into broad contact with the clearance face, as shown in **Fig. 13**. In order to analyze the cutting mechanism with the broad contact between the clearance face and the machined surface, this study proposes a model as shown in **Fig. 15**.

This model considers two forces R_r and R_c. R_r is the resultant force acting on the rake face, while R_c is the resultant force acting on the clearance face. The normal stresses acting on the respective faces during cutting can be expected to be high. It has been reported in the literature that the friction coefficient between rubber and metal becomes constant at a high pressure of approximately 40 MPa [26]. Considering the severe stresses state on the rake and clearance faces during cutting as shown in **Fig. 13**, it can be assumed that the friction angle at the interface between the rake face and the chip and the friction angle at the interface between the clearance face and the machined surface are the same. On the basis of this assumption, the following equation can be established:

$$\begin{Bmatrix} R_r \\ R_c \end{Bmatrix} = \frac{1}{\cos(2\beta-\gamma-\alpha)} \begin{pmatrix} \cos(\beta-\alpha) & -\sin(\beta-\alpha) \\ -\sin(\beta-\gamma) & \cos(\beta-\gamma) \end{pmatrix} \begin{Bmatrix} FP \\ FT \end{Bmatrix} \quad \ldots \quad (3)$$

where FP and FT are the principal force and thrust force, respectively, and β is the friction angle on both the faces. This model is also based on the assumption that the force R_c does not affect the stress field in the shear zone. Hence, the shear stress of the material, τ_s, on the shear plane can be calculated as follows:

$$\tau_s = \frac{R_r}{bt_1}\cos(\phi+\beta-\gamma)\sin\phi - \rho V^2 \frac{\cos\gamma\sin\phi}{\cos(\phi-\gamma)} \quad (4)$$

where ρ is the density of NR (ρ = 1556 kg/m^3). The second term on the right side of Eq. (4) represents the effect of the inertia force that originates from the change in momentum in the shear zone.

The value of β is a parameter in this model. As described above, the friction angle can be expressed only in terms of the rake angle. Some cutting equations have been proposed to describe the interrelation of the shear angle, the friction angle at the tool-chip interface, and the friction angle at the shear plane. Among these equations, Merchant's theory and Lee-Shaffer's theory are most commonly used in metal cutting. Noting Eq. (1), the value of β becomes zero when Merchant's theory [23] is adopted:

$$\phi = \frac{\pi}{4} - \frac{1}{2}(\beta-\gamma) \equiv \frac{\pi}{4} + \frac{\gamma}{2} \quad \therefore \beta = 0 \quad . . \quad (5)$$

On the other hand, the value of β is calculated as half of the value of the rake angle γ when Lee-Shaffer's theory [23] is adopted:

$$\phi = \frac{\pi}{4} - (\beta-\gamma) \equiv \frac{\pi}{4} + \frac{\gamma}{2} \quad \therefore \beta = \frac{\gamma}{2} \quad . . . \quad (6)$$

A general relation between $(\beta-\gamma)$ and ϕ lies between the relation described by Merchant's theory and the relation described by Lee-Shaffer's theory. Hence, there exists an appropriate range for β Therefore, in this study, the stress field of the shear zone was evaluated by varying the value of β from 0° to 20°.

Figure 16 shows the changes in the resultant forces R_r and R_c with changing cutting speed. To calculate the changes in R_r and R_c continuously with respect to changes in the cutting speed, the curves shown in **Fig. 14** were used. The solid lines indicate the resultant force R_r acting on the rake face, whereas the broken lines indicate the resultant force R_c acting on the clearance face. Both of these forces increase rapidly with the cutting speed, regardless of the friction angle. A high rake angle reduces R_r greatly. In contrast, the magnitude of the resultant force R_c does not seem to be affected by the rake angle.

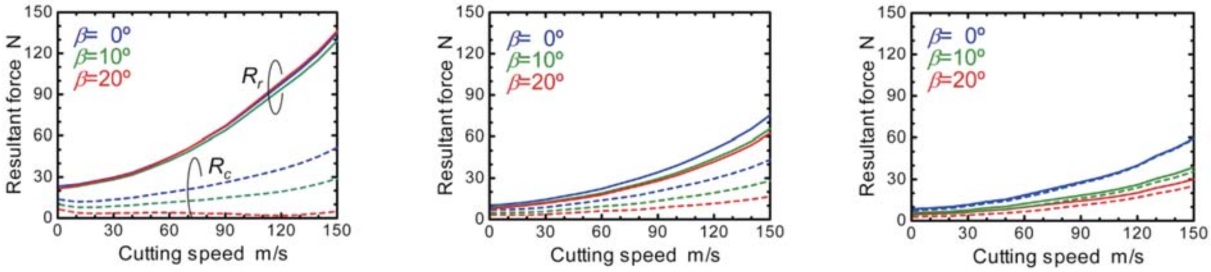

(a) $\gamma = 0°$ (b) $\gamma = 20°$ (c) $\gamma = 50°$

Fig. 16. Changes in resultant cutting forces R_r and R_c with cutting speed.

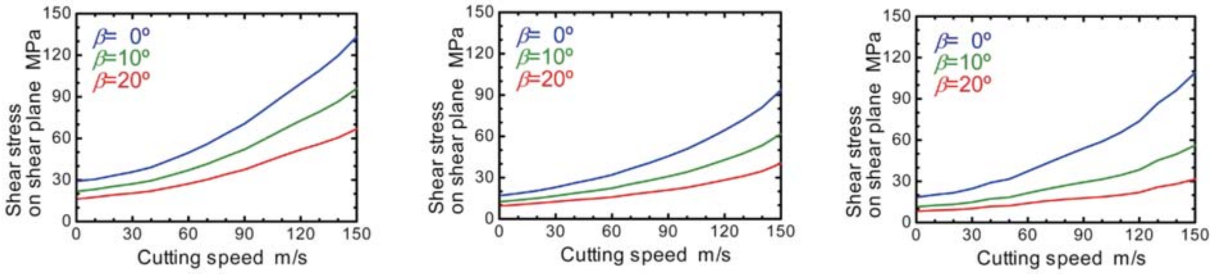

(a) $\gamma = 0°$ (b) $\gamma = 20°$ (c) $\gamma = 50°$

Fig. 17. Change in shear stress on the shear plane with cutting speed.

Figure 17 shows the change in the shear stress on the shear plane τ_s as a function of the cutting speed using Eq. (4). The shear stress rises sharply as the cutting speed increases, regardless of the rake angle. Although the calculations made in this study involve some assumptions, the cause of the increase in the shear stress can be explained by the phenomenon of a high deformation rate elevating the viscous drag of a material.

4. Discussion

Summarizing the experimental results, the cutting state of NR can be illustrated as shown in **Fig. 18**. Chipping defects occur at the entry edge of the workpiece, as shown in **Fig. 18(a)**, whereas an uncut portion remains at the exit edge, as shown in **Fig. 18(b)**. The use of a high rake angle is able to eliminate the occurrence of chipping defects, and high-speed cutting can also reduce the occurrence of chipping defects. However, the uncut portion cannot be removed. Tear defects occur when the cutting speed is slow and the rake angle is small. As **Fig. 18(c)** shows, the material near the cutting edge deforms largely toward the free surface side. Because of the large deformation with side flow, the material near both of the side edges is hardly cut. After the cutting edge passes through, the deformation recovers elastically. During recovery, the material comes into broad contact with the clearance face. As a result, the cross section of the machined surface along the width of the workpiece becomes concave in shape. The principal reason for this degradation in the shape accuracy is the large viscoelastic deformation that occurs in the shear zone. **Fig. 18(c)** suggests that if the large side flow of the material on the rake face can be restricted, the degradation in the shape accuracy of the machined surface can be reduced.

As described before, at a certain rake angle, the shear strain γ_s on the shear plane is constant regardless of the cutting speed. On the other hand, the shear stress τ_s on the shear plane increases with the cutting speed. This means that in the shear zone, the apparent stiffness of the workpiece material is enhanced as the cutting speed increases. Despite the increase in the stiffness caused by high-speed cutting, cutting at higher speeds actually deteriorates the shape accuracy of the machined surface, as shown in **Figs. 11** and **12**. One of the reasons for this seems to be related to the propagation of a stress wave in the shear zone. The speed of the stress wave, c, in the workpiece can be estimated as follows:

$$c = \sqrt{\frac{E}{\rho}} \quad \dots\dots\dots\dots\dots\dots (7)$$

where E is the Young's modulus, and ρ is the density. The value of the Young's modulus can be estimated from the Shore A hardness number Sh_A using the following equation [22]:

$$E = \frac{(1-\nu^2)(F_0 + KSh_A)}{2Rd(100 - Sh_A)} \quad \dots\dots\dots (8)$$

where ν is the Poisson's ratio. In this study, a value of 0.5 was assumed for the Poisson's ratio, and the following values were assumed for the other parameters in Eq. (8): $R = 0.395$ mm, $F_0 = 0.549$ N, $K = 0.07512$ N/Sh_A, and $d = 0.025$ mm/Sh_A. These are the constants for the type A durometer defined by ASTM D 2240. Substituting the value of the Shore A hardness number of NR ($Sh_A = 69$) into Eq. (8) yields a value of a 7.02 MPa for the Young's

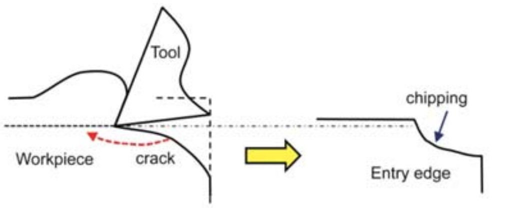

(a) Development of chipping defect at the beginning of cutting

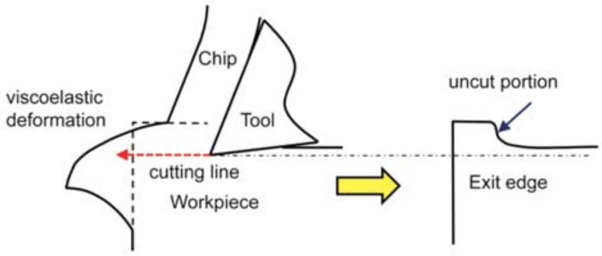

(b) Development of uncut at the end of cutting

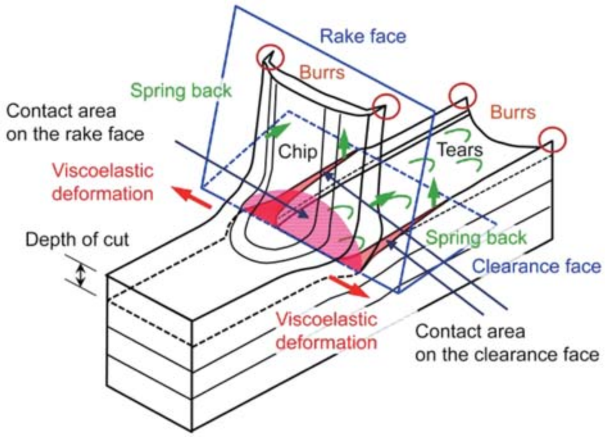

(c) Whole view

Fig. 18. Schematic depiction of cutting state of NR.

modulus. Thus, from Eq. (7), the speed of the stress wave is calculated to be 67.2 m/s. Considering the cutting model illustrated in **Fig. 15** and using Eq. (1), the shear speed on the shear plane, V_s, can be calculated as follows:

$$V_s = \frac{\cos\gamma}{\cos(\phi-\gamma)}V = 2V\cos\left(\frac{\pi}{4}+\frac{\gamma}{2}\right) \quad . \ . \ . \ (9)$$

If the shear speed V_s exceeds the speed c of the stress wave, shock waves will be developed. Therefore, the cutting speed at which the shear speed corresponds to the speed of the stress wave is defined in this study as a critical cutting speed V_{crt}. The critical cutting speed can be calculated as follows:

$$V_{crt} = \frac{1}{2\cos\left(\frac{\pi}{4}+\frac{\gamma}{2}\right)}c \quad . \ . \ . \ . \ . \ . \ . \ . \ (10)$$

Figure 19 shows the relation between the rake angle and the critical cutting speed, calculated using Eq. (10). A cutting speed of less than 40 m/s is below the critical cutting speed for any rake angle. When the cutting speed is 100 m/s, shock waves will be generated in the shear zone regardless of the rake angle. Shock waves produce high levels of hydrostatic stresses. To reduce the hydrostatic stresses generated in the shear zone, the material deforms substantially to flow toward both sides. This results in the considerable side flow [17]. As **Fig. 12** shows, the accuracy of the cross section of the machined surface at a cutting speed of 130 m/s is lower than that at a cutting speed of 30 m/s. This experimental result supports the explanation that shock waves degrade the shape accuracy of the machined surface.

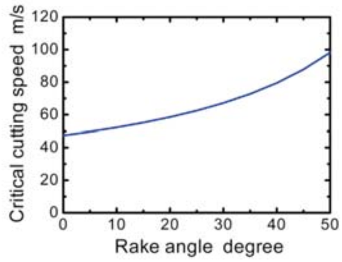

Fig. 19. Change in critical cutting speed with rake angle.

Increasing cutting speed is effective for NR cutting. However, depending on the rake angle, there is a critical cutting speed that should not be exceeded to increase the shape accuracy of the machined surface and improve the cutting performance of NR.

5. Conclusions

Orthogonal cutting experiments of NR were conducted at cutting speeds ranging from 1.0 m/s to 141.1 m/s and at rake angles of 0°, 20° and 50°. The obtained data were used to examine the contributions of high-speed cutting and a high rake angle to the cutting performance of NR. The following conclusions were drawn from the results of this study:

(1) A high rake angle such as 50° is favorable because it produces a flat machined surface without tears. However, a high rake angle will make the thrust force negative at low cutting speeds, and it cannot eliminate the presence of an uncut portion of the material at the exit edge.

(2) For tools with rake angles of less than 50°, high-speed cutting is effective in eliminating of tear defects on the machined surface and chipping defects at the entry edge of the workpiece. When the cutting speed is approximately 30 m/s, the shape accuracy of the machined surface is improved significantly. This is attributable to the phenomenon of high-speed cutting enhancing the apparent stiffness of the material in the shear zone by increasing the viscous drag.

(3) The speed of the stress wave for NR is estimated to be 67.2 m/s. The cutting speed at which the shear speed in the shear zone corresponds to the speed of the stress wave is defined in this study as the critical cutting speed. This critical cutting speed depends on the rake angle. A cutting speed faster than the critical speed is undesirable because shock waves will be

generated in the shear zone.

The results of this study suggest that restricting the large side flow on the rake face would be more effective in improving the performance of NR cutting than increasing the cutting speed or rake angle.

References:

[1] G. Heinrich, M. Kluppel, and T. A. Vilgis, "Reinforcement of elastomers," Current Opinion in Solid State and Materials Science, Vol.6, pp. 195-203, 2002.

[2] J.-H. Kim and H.-Y. Jeong, "A study on the material properties and fatigue life of natural rubber with different carbon blacks," Int. J. of Fatigue, Vol.27, pp. 263-272, 2005.

[3] L. Laiarinandrasana, A. Jean, D. Jeulin, and S. Forest, "Modelling the effects of various contents of fillers on the relaxation rate of elastomers," Materials and Design, Vol.33, pp. 75-82, 2012.

[4] H. Nabil, H. Ismail, and A. R. Azura, "Compounding, mechanical and morphological properties of carbon-black-filled natural rubber/recycled ethylenepropylene-diene-monomer (NR/R-EPDM) blends," Polymer Testing, Vol.32, pp. 385-393, 2013.

[5] J.-B. Le Cam, B. Huneau, and E. Verron, "Fatigue damage in carbon black filled natural rubber under uni- and multiaxial loading conditions," Int. J. of Fatigue, Vol.52, pp. 82-94, 2013.

[6] A. Nimpaiboon, S. Amnuaypornsri, and J. Sakdapipanich, "Influence of gel content on the physical properties of unfilled and carbon black filled natural rubber vulcanizates," Polymer Testing, Vol.32, pp.1135-1144, 2013.

[7] J. Diani, B. Fayolle, and P. Gilormini, "A review on the Mullins effect," European Polymer J., Vol.45, pp. 601-612, 2009.

[8] R. Nayak, R. Shetty, and S. Shetty, "Experimental and Finite Element Analysis on Chip Formation Mechanism in Machining of Elastomers," Bonfring Int. J. of Industrial Engineering and Management Science, Vol.2, No.2, pp. 10-13, 2012.

[9] J. Yan and J. S. Strenkowski, "A finite element analysis of orthogonal rubber cutting," J. of Materials Processing Technology, Vol.174, pp. 102-108, 2006.

[10] Y. Kakinuma, N. Yasuda, and T. Aoyama, "Micromachining of soft polymer material applying cryogenic cooling," J. of Advanced Mechanical Design, Systems, and Manufacturing, Vol.2, No.4, pp. 560-569, 2008.

[11] V. G. Dhokia, S. T. Newman, P. Crabtree, and M. P. Ansell, "A process control system for cryogenic CNC elastomer machining," Robotic and Computer – Integrated Manufacturing, Vol.27, pp. 779-784, 2011.

[12] R. Nayak, R. Shetty, and S. Shetty, "Experimental and Finite Element Analysis on Chip Formation Mechanism in Machining of Elastomers," Bonfring Int. J. of Industrial Engineering and Management Science, Vol.2, No.2, pp. 10-13, 2012.

[13] A. J. Shih, M. A. Lewis, and J. S. Strenkowski, "End Milling of Elastomers – Fixture Design and Tool Effectiveness for Material Removal," J. of Manufacturing Science and Engineering, Vol.126, pp. 115-123, 2004.

[14] J. Luo, H. Ding, and A. J. Shih, "Induction-heated tool machining of elastomers – part 2: chip morphology, cutting forces, and machined surfaces –," Machining Science and Technology, Vol.9, pp. 567-588, 2005.

[15] M. Jin and M. Murakawa, "High-Speed Milling of Rubber (1st Report) – Fundamental Experiments and Considerations for Improvement of Work Accuracy," J. of the Japan Society for Precision Engineering, Vol.64, No.6, pp.897-901, 1998. (in Japanese)

[16] D.-L. Chen, P.-F. Yang, and Y.-S. Lai, "A review of three-dimensional viscoelastic models with an application to viscoelasticity characterization using nanoindentation," Microelectronics Reliability, Vol.52, pp. 541-558, 2012.

[17] J. Shinozuka, M. Sando, and T. Horie, "Ultra High-Speed Cutting Experiment under the Cutting Condition that Cutting Speed Exceeds Plastic Wave Speed of Workpiece," Advanced Materials Research, Vol.325, pp. 327-332, 2011.

[18] J. Shinozuka, H. Yachi, T. Higashi, M. Sando, T. Maetani, S. Unami, and Y. Ozaki, "Effect of MnS on the cutting mechanism of powder metallurgy steel in cutting speeds ranging from 1 m/s to 150 m/s," Advanced Materials Research, Vol.565, pp. 370-375, 2012.

[19] M. Sando, T. Higashi, and J. Shinozuka, "Influence of the Heat Treatment Condition upon the High-Speed Cutting Mechanism of Aluminum Alloy A2017," J. of Advanced Mechanical Design, Systems, and Manufacturing, Vol.6, No.6, pp. 859-874, 2012.

[20] T. Higashi, M. Sando, and J. Shinozuka, "Cutting experiments in cutting speeds of up to 200 m/s with a high-speed impact cutting tester," Key Engineering Materials, Vols.523-524, pp. 1041-1046, 2012.

[21] J. Shinozuka, "Experimental investigation on the cutting mechanism of oxygen free copper in cutting speeds ranging from 1 m/s to 210 m/s," Advanced Materials Research, Vol.797, pp. 208-213, 2013.

[22] A. N. Gent, "On the relation between indentation hardness and Young's modulus," Transaction of the Institution of the Rubber Industry, Vol.34, pp. 46-57, 1958.

[23] M. C. Shaw, "Metal cutting principles," Oxford Science Publication, 1984.

[24] T. Matsumura, M. Shimada, K. Teramoto, and E. Usui, "Predictive Cutting Force Model and Cutting Force Chart for Milling with Cutter Axis Inclination," Int. J. of Automation Technology, Vol.7, No.1, pp. 30-38, 2013.

[25] H. Kiyota, F. Itoigawa, S. Endo, and T. Nakamura, "Analytical Approach for Optimization of Chamfered Cutting Tool Preparation Considering Built-Up Edge Extrusion Behavior," Int. J. of Automation Technology, Vol.7, No.3, pp. 329-336, 2013.

[26] M. Fukuda, K. Yamaguchi, "On the coefficient of friction between rubber and metal under high pressure," Bulletin of the JSME, Vol.17, No.103, pp. 157-164, 1974.

Name:
Naoki Takahashi

Affiliation:
Graduate Student, Yokohama National University

Address:
79-5 Tokiwadai, Hodogaya, Yokohama, Kanagawa 240-8501, Japan

Brief Biographical History:

2012- Graduate School, Yokohama National University

Name:
Jun Shinozuka

Affiliation:
Associate Professor, Yokohama National University

Address:
79-5 Tokiwadai, Hodogaya, Yokohama, Kanagawa 240-8501, Japan

Brief Biographical History:

1996- Assistant Professor, Tokyo Institute of Technology
2005- Lecturer, Ibaraki University
2008- Associate Professor, Yokohama National University

Main Works:

- "Influence of the Heat Treatment Condition upon the High-Speed Cutting Mechanism of Aluminum Alloy A2017," J. of Advanced Mechanical Design, Systems, and Manufacturing, Vol.6, No.6, pp. 859-874, 2012.
- "Development of Cutting Tool with Built-in Thin Film Thermocouples for Measuring High Temperature Fields in Metal Cutting Processes," ASME, J. of Manufacturing Science and Engineering, Vol.130, pp. 034501-1-034501-6, Jun. 2008.
- "Chip Breaking Analysis from the Viewpoint of the Optimum Cutting Tool Geometry Design," J. of Materials Processing Technology, Vol.62, pp. 345-351, 1996.

Membership in Academic Societies:

- Japan Society of Mechanical Engineers (JSME)
- Japan Society for Precision Engineering (JSPE)
- Japan Society for Abrasive Technology (JSAT)